Supporting Information

Dual-Functional Electrocatalyst Derived from Iron-Porphyrin-Encapsulated Metal–Organic Frameworks

Jungwon Park,†[a] Hyunjoon Lee,†[a] Young Eun Bae,†[c] Kyoung Chul Park,[a] Hoon Ji,[b] Nak Cheon Jeong,[b] Min Hyung Lee,[c] Oh Joong Kwon,*[ad] Chang Yeon Lee*[ad]*

[a] Department of Energy and Chemical Engineering, Incheon National University, Incheon 22012, Republic of Korea. Email: ojkwon@inu.ac.kr, cylee@inu.ac.kr

[b] Department of Emerging Materials Science, DGIST, Daegu 42988, Republic of Korea

[c] Department of Applied Chemistry, Kyung Hee University, Yongin, Gyeonggi 17104, Republic of Korea. Email: minhlee@khu.ac.kr

[d] Innovation Center for Chemical Engineering, Incheon National University, Incheon 22012, Republic of Korea

* Corresponding author.
E-mail address: cylee@inu.ac.kr, minhlee@khu.ac.kr, ojkwon@inu.ac.kr

† These authors contributed equally

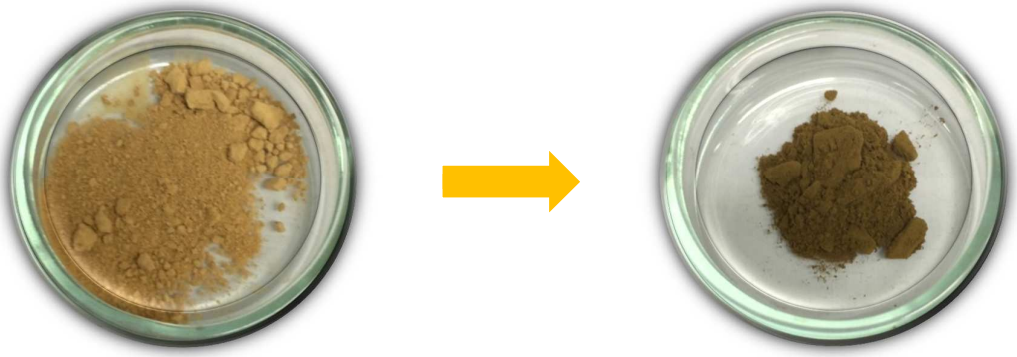

PCN-333 (Fe)

Fe-TCPP@PCN333

Figure S1. Photograph images of PCN-333 (Fe) and Fe-TCPP@PCN333.

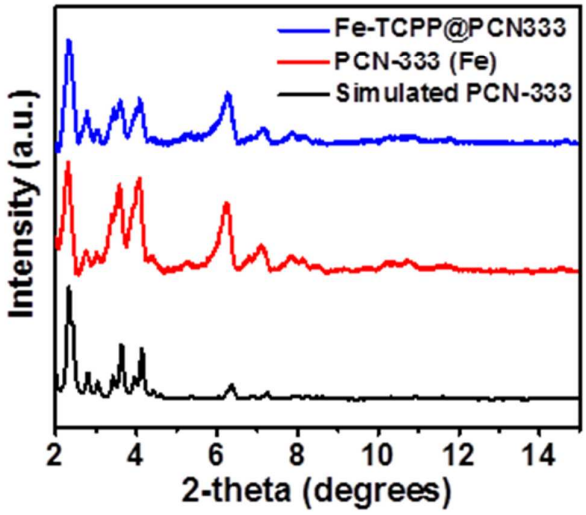

Figure S2. Powder X-ray diffraction patterns of PCN-333 (Fe) and Fe-TCPP@PCN333.

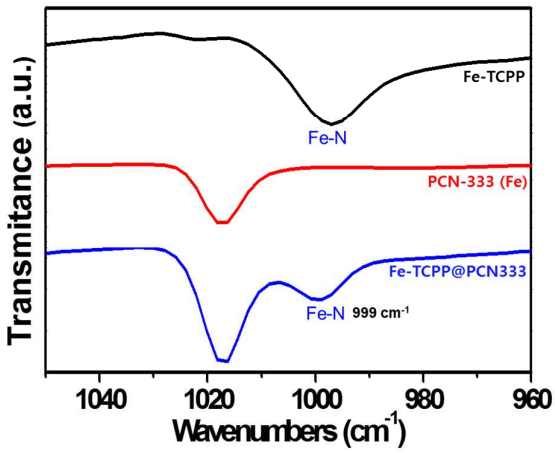

Figure S3. FTIR spectra of Fe-TCPP, PCN-333 (Fe) and Fe-TCPP@PCN333

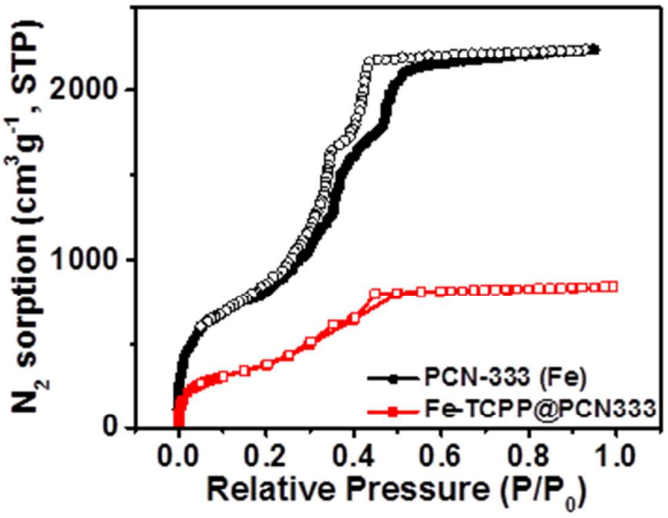

Figure S4. N_2 adsorption-desorption isotherms for PCN-333 (Fe) and Fe-TCPP@PCN333

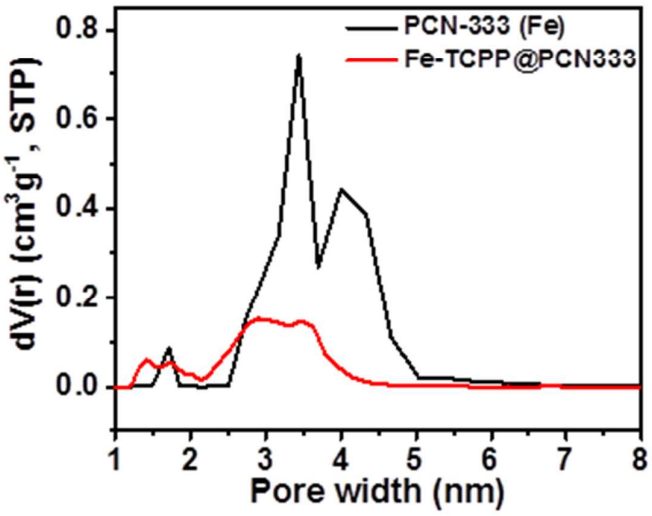

Figure S5. DFT pore size distribution for PCN-333 (Fe) and Fe-TCPP@PCN333 obtained from the N_2 isotherm measured at 77 K.

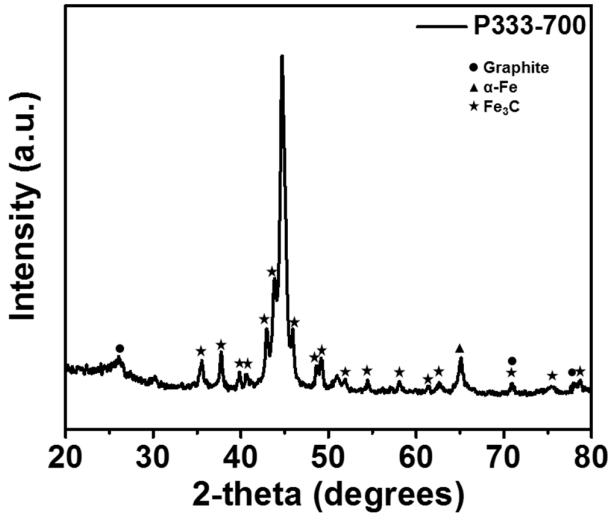

Figure S6. Powder X-ray diffraction pattern of P333-700.

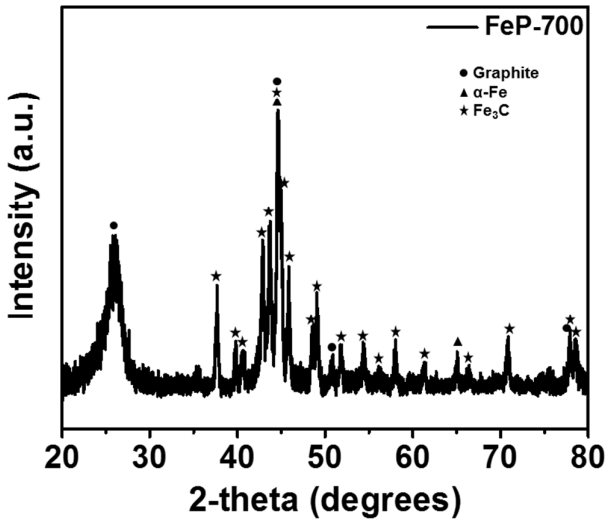

Figure S7. Powder X-ray diffraction pattern of FeP-700.

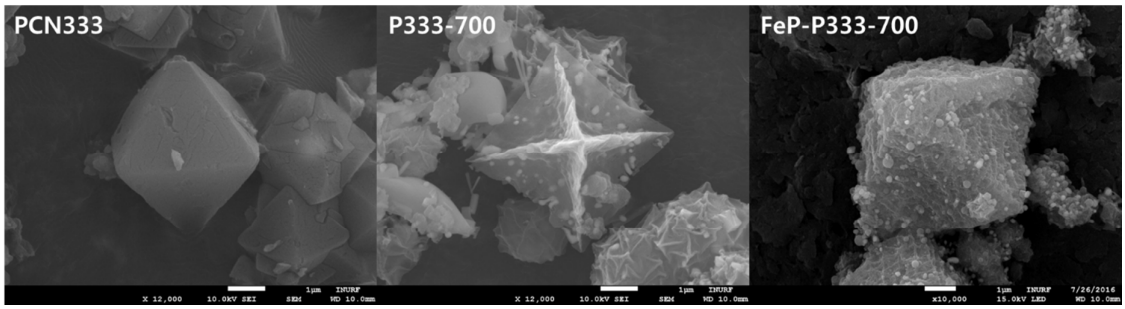

Figure S8. SEM image of PCN-333 (Fe), P333-700 and FeP-P333-700

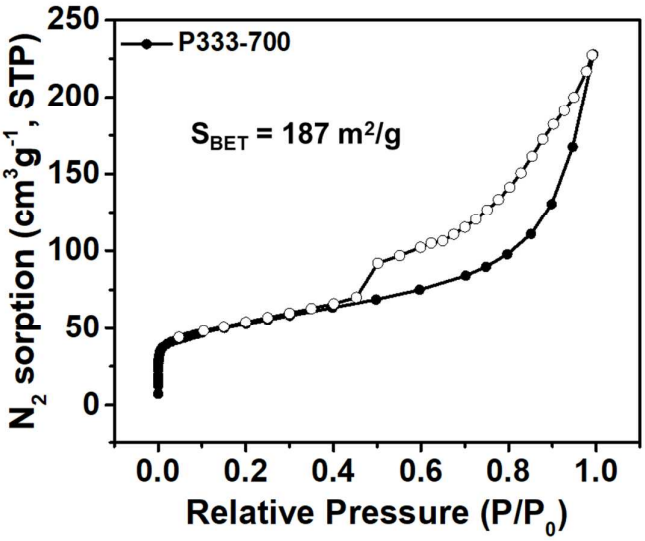

Figure S9. N_2 adsorption–desorption isotherms of P333-700.

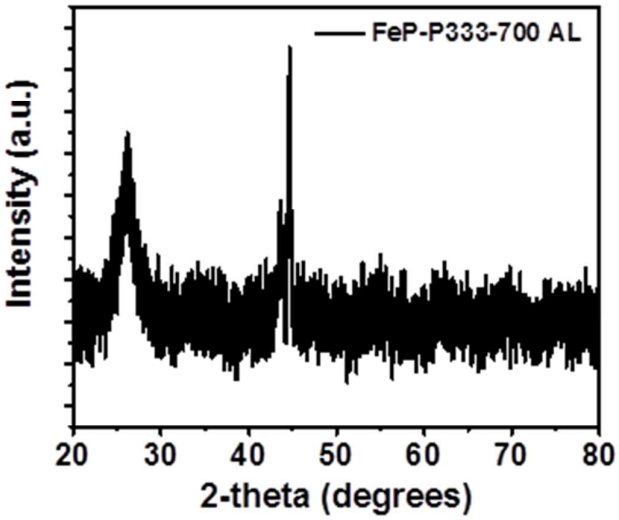

Figure S10. Powder X-ray diffraction pattern of FeP-P333-700 AL.

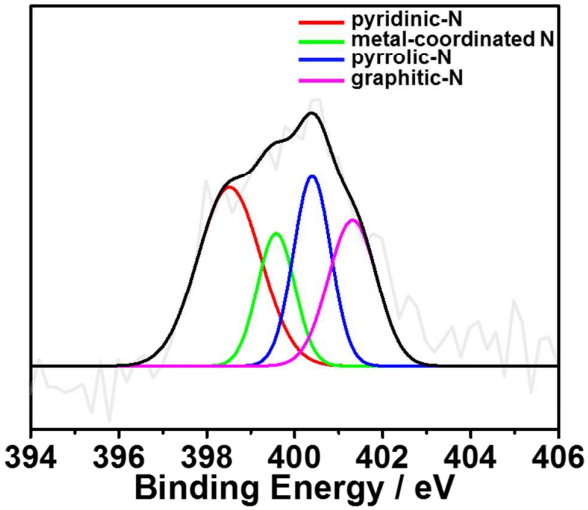

Figure S11. N 1s XPS spectra of FeP-P333-700 AL.

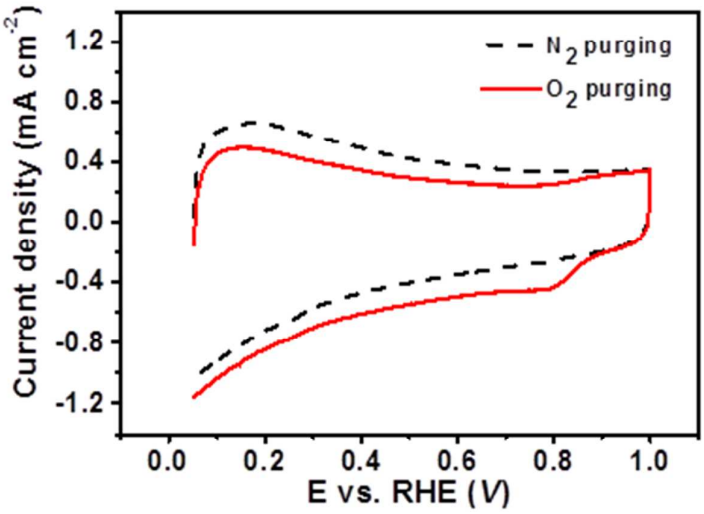

Figure S12. CVs of P333-700 in N_2 and O_2-saturated 0.1 M aqueous KOH electrolyte solutions at scan rate of 20 mVs^{-1}

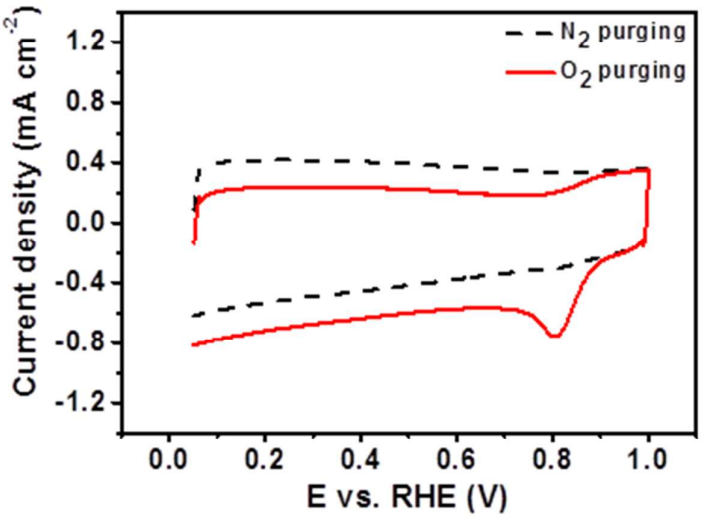

Figure S13. CVs of FeP-P333-700 AL in N_2 and O_2-saturated 0.1 M aqueous KOH electrolyte solutions at scan rate of 20 mVs^{-1}.

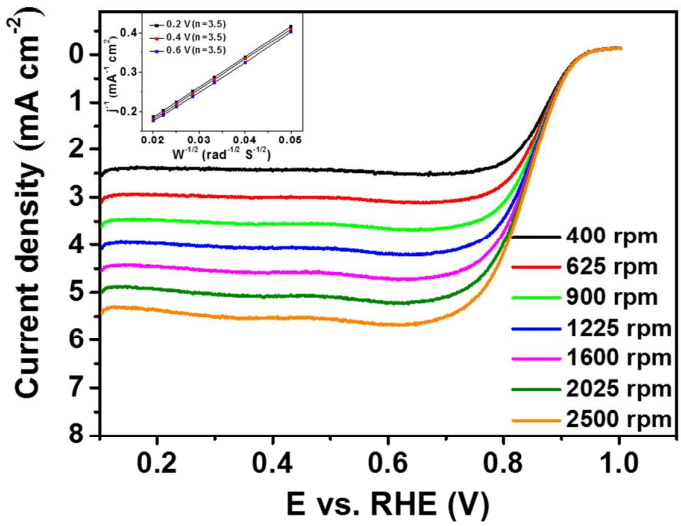

Figure S14. RDE LSVs curves of FeP-P333-700 AL at various speeds; inset shows corresponding Koutecky-Levich plots (J^{-1} vs $rpm^{-1/2}$)

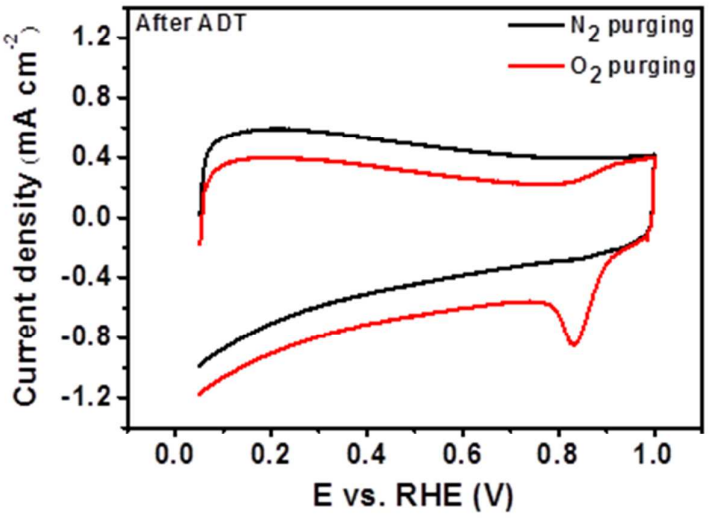

Figure S15. CVs of After ADT FeP-P333-700 in N_2 and O_2-saturated 0.1 M aqueous KOH electrolyte solutions at scan rate of 20 mVs^{-1}

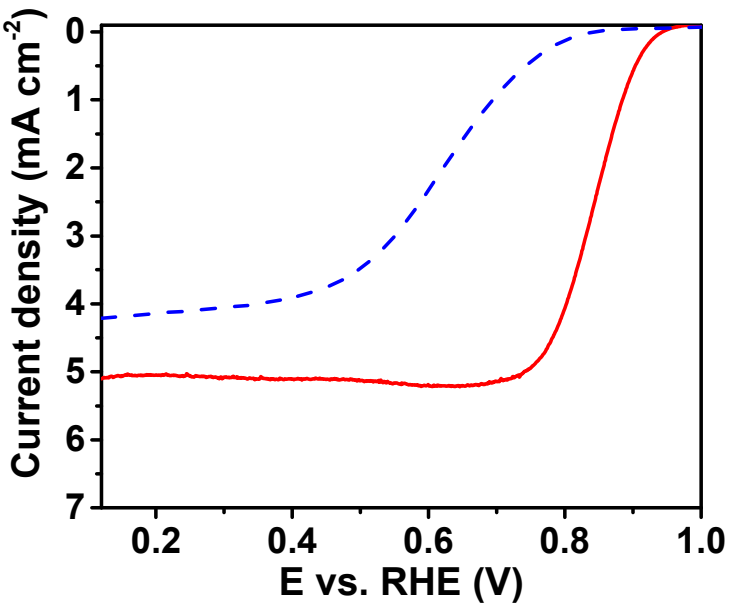

Figure S16. LSV curves of FeP-P333-700 (red solid line) and catalyst derived from physical mixture of metalloporphyrin and PCN-333 (blue dashed line) at a rotation rate of 1600 rpm in O_2-saturated 0.1 M KOH solution

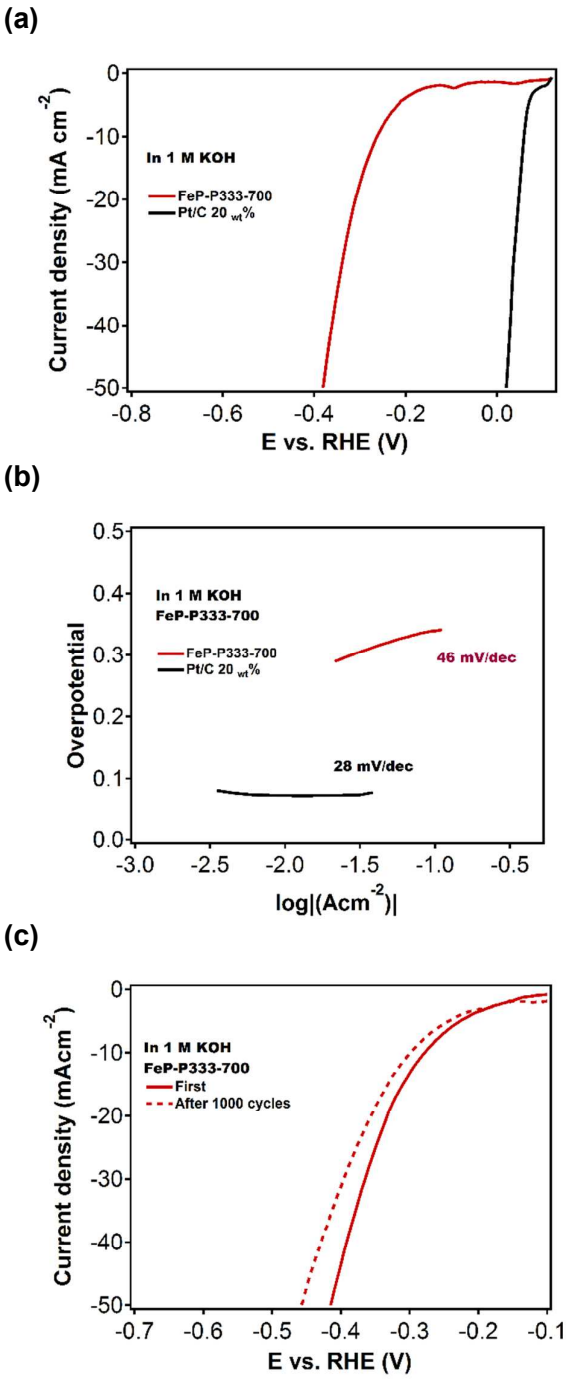

Figure S17. Electrochemical characterization of electrocatalysts FeP-P333-700 in basic electrolyte (1 M KOH, pH 14). (a) Polarization curves and (b) corresponding Tafel plots obtained from the polarization curves. (c) Durability test using consecutive 1000 cycles in 1 M KOH electrolyte with sweeping potential from -0.2 V to -1.0 V vs RHE .

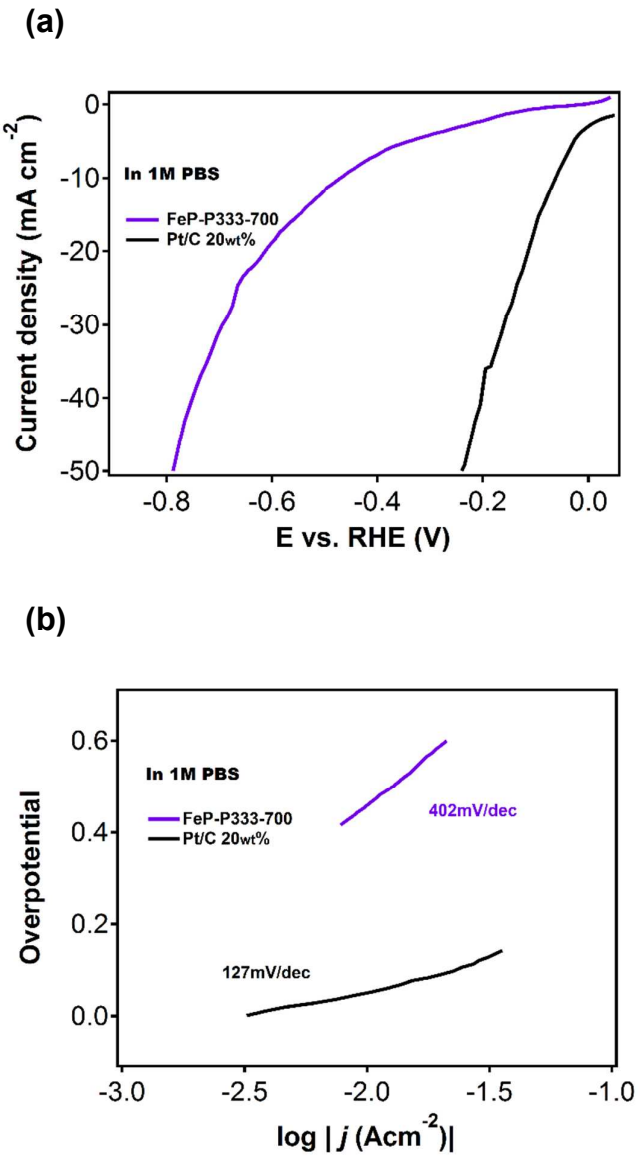

Figure S18. Electrochemical characterization of electrocatalysts FeP-P333-700 in neutral electrolyte (1 M PBS, pH 7). (a) Polarization curves and (b) corresponding Tafel plots obtained from the polarization curves.

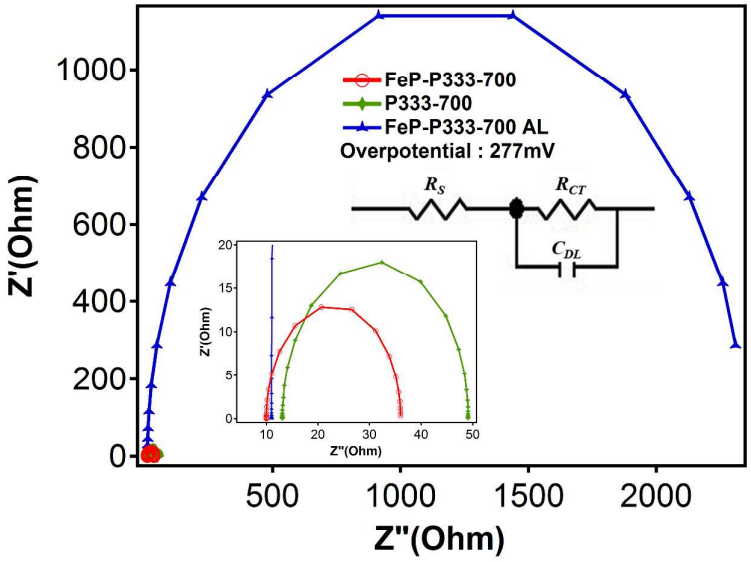

Figure S19. Nyquist plots of electrocatalysts that are fitted to the equivalent circuit shown in the inset.

Table S1. Impedance parameters of catalysts.

samples	R_S (Ω)	C_{DL} (mF)	R_{CT} (Ω)
FeP-P333-700	9.99	0.73503	26.04
P333-700	13.12	0.06535	36.01
FeP-P333-700 AL	11	0.85875	2334

Table S2. Catalytic performance comparison of catalysts in different pH condition.

Overpotential (E vs. RHE)	**FeP-P333-700**		**Pt/C 20$_{wt}$%**	
	10 mA/cm^2	100 mA/cm^2	10 mA/cm^2	100 mA/cm^2
pH 0.1	0.207	0.357	0.017	0.147
pH 7	0.420	0.890	0.065	0.450
pH 14	0.301	0.480	0.057	0.022
Overpotential (E vs. RHE)	**P333-700**		**FeP-P333-700 AL**	
	10 mA/cm^2	100 mA/cm^2	10 mA/cm^2	100 mA/cm^2
pH 0.1	0.237	0.412	0.527	0.727

Table S3. Comparison of half-wave potential of the Fe_3C based non-precious electrocatalysts in 0.1 M KOH electrolyte reported in the literatures.

Catalyst	Half-wave potential (V vs. RHE)	Electrolyte	Reference
FeMo Carbide/NG-800	0.642	0.1 M KOH	S1
Fe-W-C	0.727	0.1 M KOH	S2
Carbonized porous cubes	0.78	0.1 M KOH	S3
Fe_3C-GNRs	0.78	0.1 M KOH	S4
Fe-C/NG-10%-700-AL	0.793	0.1 M KOH	S5
Fe_3C@N-C-900	0.806	0.1 M KOH	S6
Fe_3C@NG-800-0.2	0.81	0.1 M KOH	S7
Fe-N-GNFs	0.824	0.1 M KOH	S8
Fe_3C@NCNTs-800	0.825	0.1 M KOH	S9
Fe_3C/b-NCNT	0.83	0.1 M KOH	S10
Fe_3C/C-800	0.83	0.1 M KOH	S11
Fe/Fe_3C@C/RGO	0.83	0.1 M KOH	S12
Fe/Fe_3C/melamine/ N-KB	0.83	0.1 M KOH	S13
Fe-N-CNFs	0.832	0.1 M KOH	S14
Fe_3C@N-CNT assemblies	0.85	0.1 M KOH	S15
Fe_3C/NG-800	0.86	0.1 M KOH	S16
FeP@P333-700	0.843	0.1 M KOH	This work

Reference :

[S1] Chen, M.; Liu, J.; Zhou, W.; Lin, J.; Shen, Z. Nitrogen-doped Graphene-Supported Transition-Metals Carbide Electrocatalysts for Oxygen Reduction Reaction. *Sci. Rep.* **2015**, *5*, 10389-10398.

[S2] Yang, J.; Xie, Y.; Wang, R.; Jiang, B.; Tian, C.; Mu, G.; Yin, J.; Wang, B.; Fu, H. Synergistic Effect of Tungsten Carbide and Palladium on Graphene for Promoted Ethanol Electrooxidation. *ACS Appl. Mater. Interfaces* **2013**, *5*, 6571–6579.

[S3] Wu, Y.; Zhao, S.; Zhao, K.; Tu, T.; Zheng, J.; Chen, J.; Zhou, H.; Chen, D.; Li, S. Porous Fe-N_x/C Hybrid Derived from Bi-Metal Organic Frameworks as High Efficient Electrocatalyst for Oxygen Reduction Reaction. *J. Power Sources* **2016**, *311*, 137-143.

[S4] Fan, X.; Peng, Z.; Ye, R.; Zhou, H.; Guo, X. M_3C (M: Fe, Co, Ni) Nanocrystals Encased in Graphene Nanoribbons: An Active and Stable Bifunctional Electrocatalyst for Oxygen Reduction and Hydrogen Evolution Reactions. *ACS Nano* **2015,** *9*, 7407–7418.

[S5] Xue, J.; Zhao, L.; Dou, Z.; Yang, Y.; Guan, Y.; Zhu, Z.; Cui, L. Nitrogen-Doped 3D Porous Carbons with Iron Carbide Nanoparticles Encapsulated in Graphitic Layers Derived from Functionalized MOF as an Efficient Noble-Metal-Free Oxygen Reduction Electrocatalysts in Both Acidic and Alkaline Media. *RSC Adv.* **2016**, *6*, 110820–110830.

[S6] Liu, Y.-L.; Xu X.-Y.; Sun, P.-C.; Chen, T.-H. N-Doped Porous Carbon Nanosheets with Embedded Iron Carbide Nanoparticles for Oxygen Reduction Reaction in Acidic Media. *Int. J. Hydrogen Energy* **2015**, *40*, 4531-4539.

[S7] Jiang, H.; Yao, Y.; Zhu, Y.; Liu, Y.; Su, Y.; Yang, X.; Li, C. Iron Carbide Nanoparticles Encapsulated in Mesoporous Fe–N-Doped Graphene-Like Carbon Hybrids as Efficient Bifunctional Oxygen Electrocatalysts. *ACS Appl. Mater. Interfaces* **2015**, *7*, 21511–21520.

[S8] Wu, J.; Ma, L.; Yadav, R. M.; Yang, Y.; Zhang, X.; Vajtai, R.; Lou, J.; Ajayan, P. M.

Nitrogen-Doped Graphene with Pyridinic Dominance as a Highly Active and Stable Electrocatalyst for Oxygen Reduction. *ACS Appl. Mater. Interfaces* **2015**, *7*, 14763–14769.

[S9] Zhong, G.; Wang, H.; Yu, H.; Peng, F. Nitrogen Doped Carbon Nanotubes with Encapsulated Ferric Carbide as Excellent Electrocatalyst for Oxygen Reduction Reaction in Acid and Alkaline Media. *J. Power Sources* **2015**, *286*, 495-503.

[S10] Aijaz, A.; Masa, J.; Rösler, C.; Antoni, H.; Fischer, R. A.; Schuhmann, W.; Muhler, M. MOF-Templated Assembly Approach for Fe_3C Nanoparticles Encapsulated in Bamboo-Like N-Doped CNTs: Highly Efficient Oxygen Reduction under Acidic and Basic Conditions. *Chem. Eur. J.* **2017**, *23*, 1–7.

[S11] Hu, Y.; Jensen, J. O.; Zhang, W.; Cleemann, L. N.; Xing, W.; Bjerrum, N. J.; Li, Q. Hollow Spheres of Iron Carbide Nanoparticles Encased in Graphitic Layers as Oxygen Reduction Catalysts. *Angew. Chem. Int. Ed.* **2014**, *53*, 3675-3679.

[S12] Hou, Y.; Huang, T.; Wen, Z.; Mao, S.; Cui, S.; Chen, J. Metal-Organic Framework-Derived Nitrogen-Doped Core-Shell-Structured Porous Fe/Fe_3C@C Nanoboxes Supported on Graphene Sheets for Efficient Oxygen Reduction Reactions. *Adv. Energy Mater.* **2014**, *4*, 1400337.

[S13] Lee, J.-S.; Park, G. S.; Kim, S. T.; Liu, M.; Cho, J. A Highly Efficient Electrocatalyst for the Oxygen Reduction Reaction: N-Doped Ketjenblack Incorporated into Fe/Fe_3C-Functionalized Melamine Foam. *Angew. Chem. Int. Ed.* **2013**, *52*, 1026-1030.

[S14] Wu, Z.-Y.; Xu, X.-X.; Hu, B.-C.; Liang, H.-W.; Lin, Y.; Chen, L.-F.; Yu, S. H. Iron Carbide Nanoparticles Encapsulated in Mesoporous Fe-N-Doped Carbon Nanofibers for Efficient Electrocatalysis. *Angew. Chem. Int. Ed.* **2015**, *54*, 8179-8183.

[S15] Guan, B. Y.; Yu, L.; Lou, X. W. A Dual-Metal–Organic-Framework Derived Electrocatalyst for Oxygen Reduction. *Energy Environ. Sci.* **2016**, *9*, 3092-3096.

[S16] Xiao, M.; Zhu, J.; Feng, L.; Liu, C.; Xing, W. Meso/Macroporous Nitrogen-Doped Carbon Architectures with Iron Carbide Encapsulated in Graphitic Layers as an Efficient and Robust Catalyst for the Oxygen Reduction Reaction in Both Acidic and Alkaline Solutions. *Adv. Mater.* **2015**, *27*, 2521-2527.